# Investigation of Interior Permanent Magnet Synchronous (IPMS) Machine Applications in Electrical Vehicle Engine Industry

Nihat Pamuk [1]

[1] *Zonguldak Bulent Ecevit University, Faculty of Engineering, Electrical and Electronics Engineering, Zonguldak, Turkey*

***Abstract*** **–This paper discusses the selection of an interior permanent magnet synchronous machine and converter for a 100V-200V DC, 100-400 Hz, 150-175 Nm, 30kW-100kW, 1550-4100 rpm electrical vehicle engine alternator. The electrical vehicle engine application requirements are outlined including the engine coupling configuration. Then the characteristics of different machines and their converters are compared through a competitive trade-off study framed by the alternator requirements; direct-drive induction, variable-reluctance, surface permanent magnet synchronous machine, and interior permanent magnet synchronous machine are all considered. The results of the study indicate that the interior permanent magnet synchronous machine is a potentially superior candidate, and so this machine is selected for further investigation. The preliminary findings are described, and the paper concludes with a discussion of current work addressing analytic design.**

***Keywords*** **– Magnetic circuit analysis, finite element analysis, electrical vehicle industry, IPMS.**

## 1. Introduction

The concept of electrical vehicles such as cars, buses, and trains used in the industry is becoming more and more attractive thanks to developing technology.

DOI: 10.18421/TEM124-04
https://doi.org/10.18421/TEM124-04

**Corresponding author:** Nihat Pamuk,
*Department of Electrical and Electronics Engineering, Zonguldak Bulent Ecevit University, Zonguldak, Turkey*
**Email:** nihatpamuk@beun.edu.tr

*Received: 09 August 2023.*
*Revised: 25 October 2023.*
*Accepted: 30 October 2023.*
*Published: 27 November 2023.*



Scientific studies in recent years have shown that electrical vehicle equipment has replaced mechanical, hydraulic, and pneumatic equipment used for propulsion and control purposes in hybrid electrical vehicles. This situation increases the operating efficiency and reliability of the electric vehicle industry and reduces the maintenance period.

For starting and generation systems, electrical transportation vehicle applications pose a special set of performance, environmental, interface, and cost criteria [1]. This paper describes one set of future requirements and proposes a system to meet those needs. The necessary conditions for beginning and generating a typical low-carbon vehicle that would be put into production between 2025 and 2030 are the basis for the system's intended use. Alternator power requirements will be greater than what the current claw-pole design can handle. Power demands on alternators will exceed the capability of the current claw-pole design when additional electrical loads are added to electrical vehicles [2]. These improvements will reduce the difference between the torque required to generate electricity and the torque required to start the engine, making combined generator systems more attractive. . This in turn suggests the consideration of different mechanical couplings between the engine and the electrical system.

This paper contrasts the attributes of four electric machine systems considering the proposed requirements through a competitive trade-off study. The interior permanent magnet synchronous machine considered here has a conventionally laminated rotor structure with magnet material buried in internal rotor cavities. The salient rotor structure enables flux-weakened operation throughout a large constant power zone, and the permanent magnet synchronous machine field aids in the production of low-speed torque [3]. The interior permanent magnet synchronous machines and their close relatives (without magnets) have received considerable interest over the last several years [4].

This study has exposed the potential for high torque and the flux-weakening capability of the interior permanent magnet synchronous machine when sufficiently high, yet realistic rotor inductance saliency ratios are attained. Saliency ratio targets used for the initial trade-off portion of this study were drawn from the results of previous work on similar structures [5].

## 2. Electrical Requirements and Engine Coupling Configuration

The attractive machine converter system options are restricted by requirements for low initial cost, high starting torque, wide constant power range during generation, long system life, high-temperature operation, and a low-voltage DC interface [6]. Electrical power is being seriously considered the preferred alternative to conventional hydraulic or pneumatic power for a variety of important accessory systems including steering and braking [7].

For this application, the assumed generating requirement is 40 kW output power at 600 rpm engine speed (idle conditions) rising to 60 kW at 6000 rpm. In addition, it is assumed that electrically actuated engine valves will be introduced into high-end vehicles before 2030 imposing an additional speed-dependent electrical load that increases linearly with engine speed, reaching 20 kW at 6000 rpm. The 65 to 70% efficiency of electrical vehicle alternators used today will be insufficient for future vehicles due to increased alternator losses, which would lead to unacceptably high cooling requirements and reduced fuel efficiency. As a result, the alternator system efficiency requirement was set at 75% (minimum) at 2500 engine rpm and 75% rated base load (i.e. 60 kW) for the combined electrical machine and converter [8]. Machine winding current density limits were set at 50 A/mm$^2$ transients during starting and 20 A/mm$^2$ steady state during generation, based on the assumption that liquid cooling will be available for the machine if necessary.

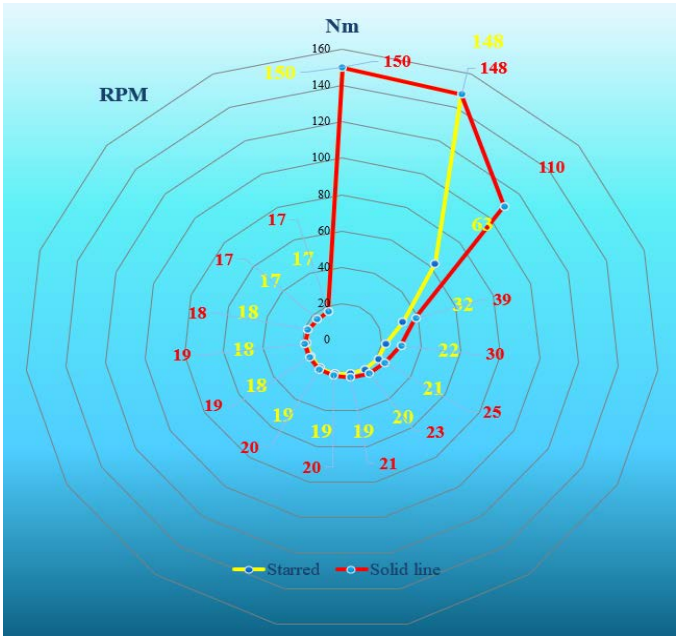


*Figure 1. Internal permanent magnet machine torques, estimated producing torque requirements, and alternator starting torques*

The vehicle electrical system voltage is assumed to increase to 80 V DC (regulated bus voltage) in comparison to the 14 V DC bus voltage used in today's vehicles. Although conventional alternators using DC brush motors produce as much as 175 Nm engine starting torque at standstill, there is no consensus among electrical vehicle experts about whether such high torque levels are required to start a large 5-liter internal combustion engine under all ambient temperature conditions (-40 $^0$C to 120 $^0$C) [9]. In another study [10], it was decided to set the engine starting torque requirement to 150 Nm up to 1900 rpm engine speed from a standstill.

The starting and generating torque requirements that occur with the speed function required for the combined alternator assembly are shown in Figure 1. There are a couple of important observations to draw from Figure 1. First, the starting torque requirement of 150 Nm at low engine speeds is significantly higher than the peak generating torque requirement of approximately 65 Nm that occurs at 600 rpm (idle conditions). On the other hand, a very major design problem for all machine technologies is the large 10:1 generating speed range from 600 to 6000 rpm over which the alternator must give high output power (> 4 kW).

Varieties of alternative configurations were considered which utilize either the same or different mechanical speed ratios between the engine and alternator machine for starting and generating operation. A direct-drive configuration was chosen in which the alternator machine is mounted concentrically with the engine output drive shaft between the engine and transmission assembly. This configuration is attractive because it uses a single speed ratio of 1:1 for both starting and generating, which eliminates the need for many mechanical components, such as the flywheel, which is now replaced by the machine rotor, as well as pulleys and belts. Due to the operational environment and electrical vehicle assembly repair limitations, an air gap of 40.23 km was chosen.

## 3. Machine Topology Comparisons

Four alternative brushless machines were evaluated as candidates for the alternator application during the initial trade-off study portion of this investigation, induction, variable reluctance machines, interior permanent magnets, and surface permanent magnets. Design studies were conducted for each of the four targeted machine types together with their associated 42V DC converters to evaluate their comparative suitability for this direct-drive alternator application. In this study, the configuration considered combines a three-phase direct-drive induction machine with a classic six-switch, full-bridge inverter implemented with power metal oxide semiconductor field effect transistor switches. Metal oxide semiconductor field effect transistors were chosen as the preferred switch in this system because of their compatibility with the low 42V DC supply voltage. The design chosen for this study adds a single switch buck converter stage between a three-phase full-bridge inverter and a regulated 42V DC bus. This approach allows the inverter input bus voltage to rise linearly with speed, reaching over 400V DC at the top engine speed of 6000 rpm.

Insulated gate bipolar transistor power switches are assumed in place of the power metal oxide semiconductor field effect transistors because of their better compatibility with the higher bus voltage. The internal permanent magnet machine is most easily distinguished from its surface permanent magnet counterpart by the fact that the internal permanent magnet machine's magnets are hidden inside the rotor. The internal permanent magnet machine is hence a "hybrid" machine by nature, with torque contributions from the magnets as well as the iron saliency created by the magnet cavities [11]. The introduction of this reluctance torque component provides the machine designer with an important degree of freedom that is very valuable in applications such as the alternator.

It is possible to operate at very wide speed ranges with continuous power, when the magnet strength and rotor saliency are properly balanced [12]. A cross-section view of a generalized four-pole internal permanent magnet machine is shown in Figure 2.

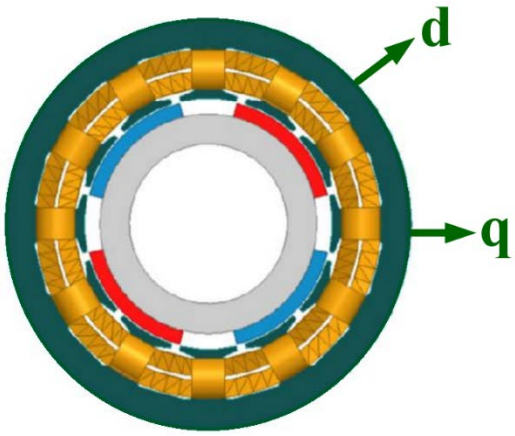


*Figure 2. Cross-section of a four-pole internal permanent magnet machine*

In this specific arrangement, the two buried magnet segments on each rotor pole are magnetized across their starting dimensions to create a four-pole field. Using poly-phase balanced sinusoidal currents to excite the stator windings, a magneto motive force wave that rotates synchronously is created. Internal permanent magnet machines can be designed with a wide range of pole numbers and rotor barrier configurations. For purposes of this discussion, the d-axis is defined as the axis of the magnet-produced field, as indicated in Figure 2.

Increasing the rotor reluctance saliency as reflected in the ratio of q-axis and d-axis stator inductances, $L_q/L_d$, provides a valuable means for reducing the cost of the internal permanent magnet machine by decreasing the required magnet cost. Some scientists have pursued axially laminated rotor designs [13] as a means of achieving higher saliency ratios. In contrast to the developed induction machine construction, the relative complexity of the internal permanent magnet machine's rotor structure constitutes a significant technological risk. Due to the incorporated magnets, the installation and magnetization procedure is more expensive and complicated during manufacturing. Alternative magnet forms include conventional block magnets, sheet magnets, or injection-mounded magnets. Further work is necessary to determine which form is most attractive for high-volume, low-cost rotor construction.

## 4. Selection of Machine Topology

Separate performance analysis models were developed for each of the four machine types.

Each of the four machine analysis routines was integrated into a recursive design optimization program which was designed to find the machine design parameters which minimized system cost while meeting all key performance requirements and design constraints. The actual optimization was accomplished in a two-stage process to narrow the design spaces for the key machine parameters, followed by a local gradient descent optimization algorithm to identify the lowest cost designs. Converter cost models were developed as a function of output current and customized for each of the four machine types. Figure 3 shows a cost graph representing the cost optimization method for each of the four possible machine types. There are several key observations that can be made based on Figure 3. First, the total projected system cost for each of the four alternative machine types is dominated by the converter cost with converter-to-machine cost ratios as high as 10:1.

Converter cost numbers presented in Figure 3 indicate that the projected cost-per-Watt is in the vicinity of US$ 0.10/Watt which is consistent with the cost of kW-class off-line switching power supplies being produced in large volumes for the computer industry.

The second observation is that the projected cost of the combined alternator system with any of the four machine technologies is too high to permit their widespread adoption in the electrical vehicle industry without significant cost reductions. The converter cost is the obvious target for such reductions, and major efforts are underway internationally to significantly reduce these costs during the coming decade. Thirdly, based on estimated system costs, the results of Figure 3 show that internal and induction permanent magnet machines are more appealing for the alternator application than surface permanent magnet machines and variable reluctance machines. Here again, it is the converter cost that makes the difference.

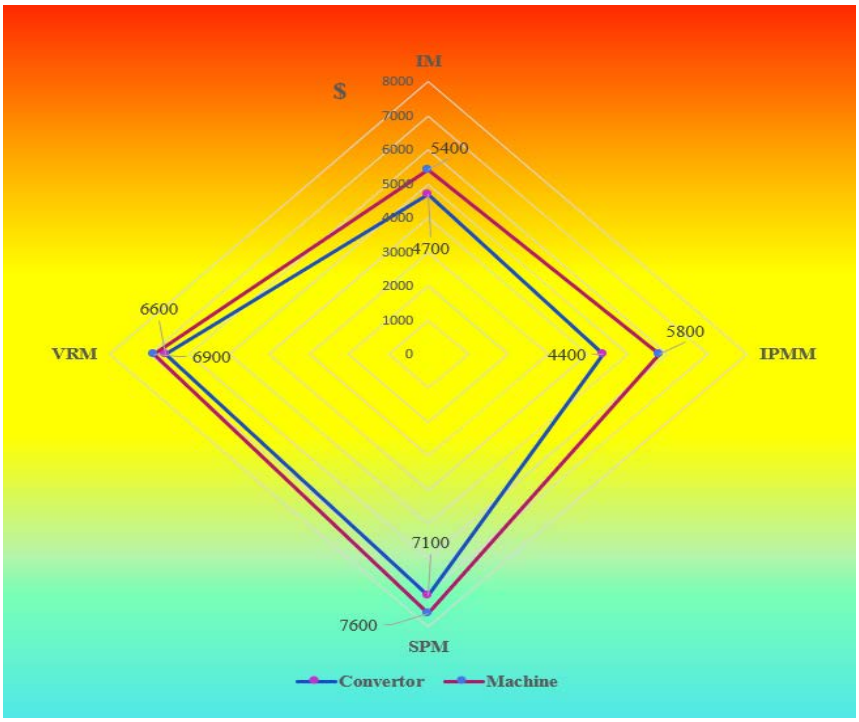


*Figure 3. Three machine systems' prices were compared for a 60 kW direct-drive alternator application*

The variable reluctance machine is penalized by the increased converter switch count due to its five-phase configuration. Since the projected system cost for the induction and internal permanent magnet machines came out to be so close, other system attributes were considered in the process of comparing the machine technologies. Due to the higher torque density anticipated for the internal permanent magnet machine, calculated machine weight also favored the internal permanent magnet machine over the induction machine by 15%. The internal permanent magnet machine's rotor is the main culprit in almost all these risk factors.

The rotor magnets present both thermal compatibility and manufacturing challenges. In addition, the impact of magnetic saturation in the rotor was recognized as a risk factor because of its potential to degrade the machine's starting torque.

## 5. Machine Analysis Techniques- Parallel Branches Equivalent Circuit Analysis for D-Axis and Q-Axis

According to this approach, the d-axis and q-axis magnetic circuits are separately modeled.

Each circuit models the flux-magneto motive force relationship in one pole of the internal permanent magnet machine, with each pole magnet and separating iron rib modeled by an individual branch in the d-axis and q-axis circuit as appropriate. The models have been designed so that the reluctance element values can vary as a function of the flux passing through them to model magnetic saturation. Enabling this nonlinear saturation feature in the d-axis and q-axis magnetic circuit requires a recursive solution, lengthening computation times. Cross-coupling magnetic effects between the two circuits are not explicitly modeled. By using *k+1* and *k* parallel branches, respectively, the d-axis and q-axis analogous circuits can be created, with *k* being the series expansion truncation order. Figure 4 depicts comparable circuit for the d-axis parallel branches.

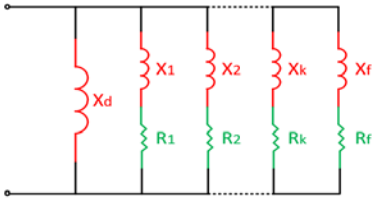


*Figure 4. D-axis parallel branches equivalent to circuit*

The q-axis parallel branches equivalent circuit is not reported, as it may be obtained from the d-axis parallel branches equivalent circuit removing the *xf, Rf* branch corresponding to field winding [14]. The parallel branches' equivalent circuit parameters are obtained with the following equations.

The equation;

$$I_{dsc} = \frac{1}{Xd} + \left(\frac{1}{X'd} - \frac{1}{Xd}\right) e^{-t/\xi' d} + T$$
$$\left[T = \left(\frac{1}{Xa} - \frac{1}{X'd}\right) . \frac{1}{k} \sum_{j=1}^{k} e^{-t/\xi_k^{j+1}}\right] \quad (1)$$

is Laplace transformed;

$$\frac{1}{Xd(p)} = \frac{1}{Xd} + \frac{p\xi_d'}{1+p\xi_d'}\left(\frac{1}{X'd} - \frac{1}{Xd}\right) + B$$
$$\left[B = \left(\frac{1}{Xa} - \frac{1}{X'd}\right) . \frac{1}{k} \sum_{j=1}^{k} \frac{p\xi_k^{j+1}}{1+p\xi_k^{j+1}}\right] \quad (2)$$

and rewritten in the classical formulation;

$$Xd(p) = Xd . \frac{\left(1+p\xi_d'\right) \prod_{j=1}^{k} \left(1+p\xi_k^{j+1}\right)}{\left(1+p\xi_{d0}'\right) \prod_{j=1}^{k} \left(1+p\xi_{k0}^{j+1}\right)} \quad (3)$$

It may be easily demonstrated the equivalence of Equation 2 with the model, equating term by term the relationships of the input terminal admittance. The sum $\xi'd0 + \xi''k0 + \xi'''k0$, the partial product sum, $\xi'd0.\xi''k0 + \xi'd0.\xi'''k0 + \xi''k0.\xi'''k0 + ....$and the product $\xi'd0.\xi''k0.\xi'''k0$ of the time constants included in Equation 3 denominator of Equation 2 can be represented as a function of reactance and temporal constants. The time constants in Equation 2 must be correlated with the time constants in each circuit of the branch. For $k = 2$ the equation system is represented by;

$$\begin{pmatrix} 1 & 1 & 1 \\ (\xi_2 + \xi_f) & (\xi_1 + \xi_f) & (\xi_1 + \xi_2) \\ (\xi_2 . \xi_f) & (\xi_1 . \xi_f) & (\xi_1 . \xi_2) \end{pmatrix} . \begin{pmatrix} \xi_{d1} \\ \xi_{d2} \\ \xi_{df} \end{pmatrix} = W \quad (4)$$

$$W = \begin{pmatrix} \xi_{d0}' + \xi_{20}' + \xi_{20}'' - \xi_1 - \xi_2 - \xi_f \\ \xi_{d0}'\xi_{20}' + \xi_{d0}'\xi_{20}'' + \xi_{20}'\xi_{20}'' - \xi_1\xi_2 - \xi_1\xi_f - \xi_2\xi_f \\ \xi_{d0}'\xi_{20}'\xi_{20}'' - \xi_1\xi_2\xi_f \end{pmatrix}$$

$$\xi_1 = \frac{L_1}{R_1}, \xi_2 = \frac{L_2}{R_2}, \xi_f = \frac{L_f}{R_f}, \xi_{d1} = \frac{L_d}{R_1}, \xi_{d2} = \frac{L_d}{R_2}, \xi_{df} = \frac{L_d}{R_f} \quad (5)$$

It is simple to confirm that $\xi_1$ is equal to, $\xi''_k$ and $\xi_2$ is equal to, $\xi'''_k$ and $\xi_f$ is equal to, $\xi'_k$. Any order *k* can be used with this approach, and the extension of equation 4 can be written as follows.

$$N_c(p) = (1 + p\xi_f) \prod_{j=1}^{k} (1 + p\xi_j) \quad (6)$$

The *j-th* derivative of $N_c(p)$, with p equal to 0, can be used to represent $S_j$, which is defined as the total of the temporal constants.

$$S_j = \frac{1}{j!} . \left.\frac{d^{(j)} N_c(p)}{dp^{(j)}}\right|_{p=0}, \quad S_{10} = \xi_{d0}' + \sum_{j=1}^{k} \xi_{k0}^{j+1} \quad (7)$$

The general formulation of Equation 4 becomes;

$$\begin{pmatrix} 1 & 1 & \cdots & 1 \\ S_1 - \xi_1 & S_1 - \xi_2 & \cdots & S_1 - \xi_f \\ S_2 - \xi_1(S_1 - \xi_1) & S_2 - \xi_2(S_1 - \xi_2) & \cdots & S_2 - \xi_f(S_1 - \xi_f) \\ S_k - \xi_1(S_{k-1} - \xi_1) & S_k - \xi_2(S_{k-1} - \xi_2) & \cdots & S_k - \xi_k(S_{k-1} - \xi_f) \end{pmatrix} . \begin{pmatrix} \xi_{d0} \\ \xi_{d1} \\ M \\ \xi_{df} \end{pmatrix} = \begin{pmatrix} S_{10} - S_1 \\ S_{20} - S_2 \\ S_{k0} - S_k \\ S_{(k+1)0} - S_{k+1} \end{pmatrix} \quad (8)$$

By omitting the branch $x_f$ $R_f$, the same approach may be used to determine the parameters of the q-axis equivalent circuit. The output of this automatic process is shown in Table 1, which is easily adaptable to any order of truncation *k*. It should be observed that while the resistances vary depending on each time constant, the sub-transient reactance maintains the same values.

*Table 1. Circuit parameters for parallel branches equivalent circuit*

| No | Circuit Parameters | | | |
|---|---|---|---|---|
| | $x_1, x_k$ | $x_f$ | $R_1, R_k$ | $R_f$ |
| 1 | $(x'_d x_a)/(x'_d - x_a)$ | $(x_d x'_d)/(x_d - x'_d)$ | $x_1/\xi''_1\omega_n$ | $1/\xi'_d\omega_n$ |
| 2 | $2.(x'_d x_a)/(x'_d - x_a)$ | $(x_d x'_d)/(x_d - x'_d)$ | $x_2/\xi''_2\omega_n$, $x_2/\xi''_2\omega_n$ | $1/\xi'_d\omega_n$ |
| k | $k.(x'_d x_a)/(x'_d - x_a)$ | $(x_d x'_d)/(x_d - x'_d)$ | $x_k/\xi''_k\omega_n$, ..., $x_k/\xi''^{k+1}_k\omega_n$ | $1/\xi'_d\omega_n$ |

### *5.1. High Order Equivalent Circuit Analysis for D-Axis*

The parallel branches equivalent circuit considers the flux coupled directly between the d-axis stator circuit and the field circuit. The parallel branches equivalent circuit may be improved to include also the flux contributed by indirect coupling through the rotor, considered as a set of small dampers. The resulting high-order d-axis equivalent circuit can be derived by introducing a preliminary external reactance $x_c$. In particular, the following parameter is computed;

$$a = \frac{\tilde{I}_{fr}}{I_0} \tag{9}$$

where $\tilde{I}_{fr}$ is the field current alternating component amplitude (50 Hz) in the three-phase short circuit test. $I_0$ is the field current reference value during the no-load machine operation. Then $x_c$ is defined as;

$$x_c \cong x_a - x_a \cdot \frac{\left(x'_d - x_a\right).a}{\left(x_d - x'_d\right) - x_a.a} \tag{10}$$

and (assuming $k = 2$) is obtained. The intermediate circuit is shown in Figure 5.

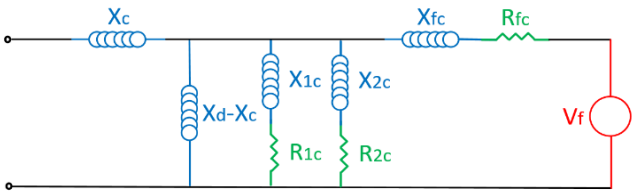


*Figure 5. Intermediate d-axis equivalent circuit*

The parallel branch equivalent parameters have been rewritten as;

$$x_{1c} = \frac{\left(2x_a - x'_d - x_a x_c - x'_d x_c\right).\left(x_a - x_c\right)}{x_a.\left(x'_d - x_a\right)}$$

$$R_{1c} = x_{1c}.\frac{1}{\xi d'''_c - \omega_n}$$

$$x_{2c} = \frac{\left(2x_a x'_d - x_a x_c - x'_d x_c\right).\left(x'_d - x_c\right)}{x'_d.\left(x'_d - x_a\right)} \tag{11}$$

$$R_{2c} = x_{2c}.\frac{1}{\xi d''_c.\omega_n}$$

$$x_{fc} = \frac{\left(x_d - x_c\right).\left(x'_d - x_c\right)}{\left(x_d - x'_d\right)}$$

$$R_{fc} = x_{fc}.\frac{1}{\xi d'_c.\omega_n}$$

Final model can be easily derived by applying the I-T transformation to the $(x_d\text{-}x_c)$ parallel branch. The I-T transformation as shown in Figure 6.

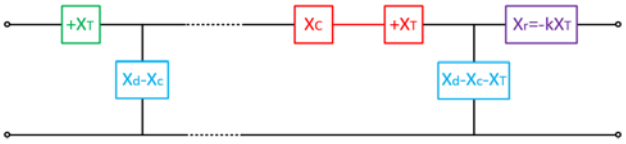


*Figure 6. I-T Transformation*

The two series reactance are hence made equal to the $x_a$ reactance;

$$x_c + x_T = x_a \tag{12}$$

and the final high order d-axis equivalent circuit is derived as shown in Figure 7. Table 2 reports all the values for the high order equivalent circuit.

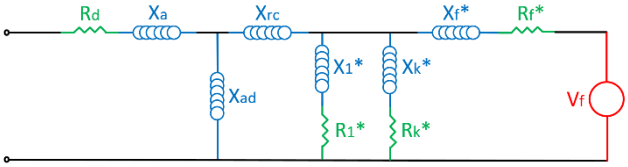


*Figure 7. D-axis high order equivalent circuit*

*Table 2. High order equivalent circuit parameters*

| Parameters | |
|---|---|
| $x_{ad} = x_d - x_a$ | $x_{rc} = (x_c - x_a).[(x_d - x_a)/(x_d - x_c)]$ |
| $x_1^* = x_{1c}.[(x_d - x_a)/(x_d - x_c)]^2$ | $R_1^* = R_{1c}.[(x_d - x_a)/(x_d - x_c)]^2$ |
| $x_2^* = x_{2c}.[(x_d - x_a)/(x_d - x_c)]^2$ | $R_2^* = R_{2c}.[(x_d - x_a)/(x_d - x_c)]^2$ |
| $x_f^* = x_{fc}.[(x_d - x_a)/(x_d - x_c)]^2$ | $R_f^* = R_{fc}.[(x_d - x_a)/(x_d - x_c)]^2$ |

A detailed analysis must be performed for the $x_{rc}$ values. The $x_{rc}$ value may be negative or positive according to the following expression;

$$x_{rc} = (-x_a) \cdot \frac{(x'_d - x_a).a}{x_a - x'_d - (x_a.a)} \cdot \left( \frac{x_d - x_a}{x_d - x_c} \right) \quad (13)$$

Being in general for a few turbo generators;

$$(x'_d - x_a) > 0 \quad , \quad (x_d - x_a) > 0 \quad , \quad (x_d - x_c) > 0 \quad (14)$$

then $x_{rc}$ is positive practically only if;

$$a > \frac{x_d - x'_d}{x_a} \quad (15)$$

A difference of an order of magnitude usually exists between the synchronous and the transient reactance.

So, the amplitude of the alternating current $\check{I}_{fr}$, with respect to $I_0$, must be of the same order. Equation 13 holds for many turbo-alternators and solid rotor synchronous machines. Anyway, $x_{rc}$ may assume also negative values. In this case, a preliminary analysis of equation 12 can be made.

### *5.2. Finite Element Analysis*

2D finite element analysis is employed to verify the predicted electromagnetic performance of the internal permanent magnet machine, providing a valuable cross-check of the magnetic circuit results. Results of the finite element analysis flux analysis are post-processed to yield torque and inductance values as functions of the stator current amplitude and orientation. Figure 8 depicts pole of permanent magnet alternator that has undergone finite element analysis and magnetic circuit analysis.

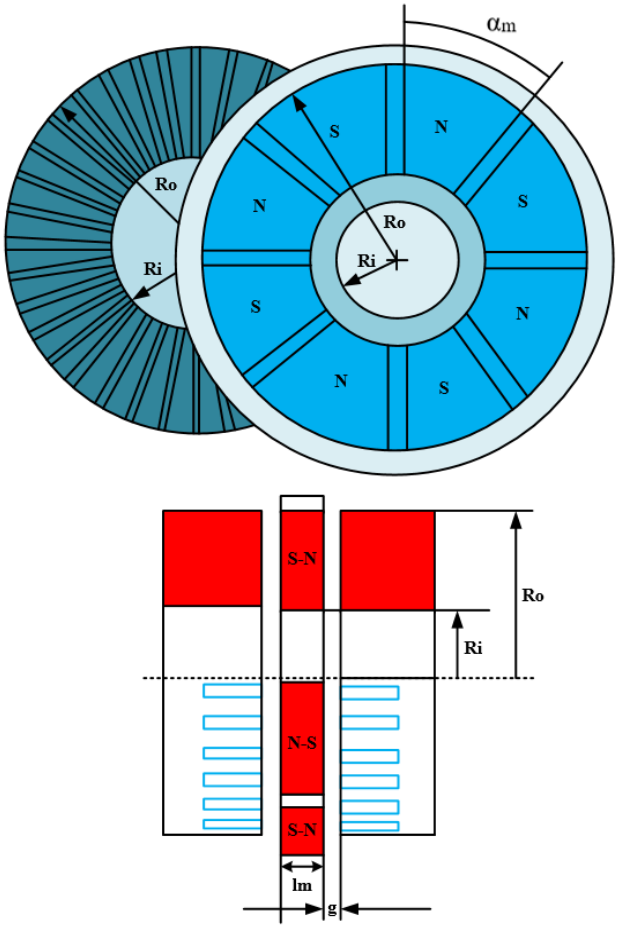


*Figure 8. Cross-section view of a machine with interior permanent magnets with two barrier layers*

This example lamination design employs two buried magnet segments per pole ($B_r$ = 0.37 T) and has a 350 mm outer stator diameter with a 114 mm core length. Analysis of this lamination design using a simplified, non-saturating, magnetic circuit predicts 240 Nm torque production with a peak stator current of 300 A oriented 53 electrical degrees ahead of the q-axis.

The predicted $L_q/L_d$ saliency ratio is approximately 9. Figure 9 shows the predicted torque vs. angle characteristic of the Figure 8 lamination design with 300 A stator current using both the magnetic circuit and finite element analysis approaches without magnetic saturation in the bulk iron.

As shown in Figure 9, the predicted torque-angle curves from the two approaches agree very closely and the d-axis current is 0 degrees. The peak predicted torque from the finite element analysis is approximately 126 Nm, which is within 10% of the preliminary torque prediction with the same current amplitude. The q-axis inductance is particularly susceptible to saturation depending on the lamination design, which can reduce the saliency ratio and degrade the reluctance torque component. Predicted machine torque is degraded, making the design unacceptable for the alternator application. This study is now focused on identifying cost-optimized internal permanent magnet machine designs that will meet the alternator requirements with the effects of magnetic saturation fully considered.

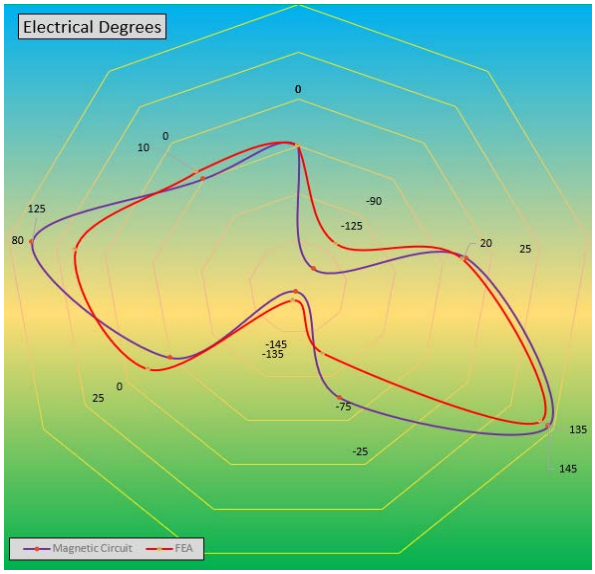


*Figure 9. Torque vs. electrical angle assuming highly permeable core and saturating bridges for magnetic circuit model*

## 6. Conclusion

The direct-drive mechanical configuration was selected for this study because of the long-term advantages it offers for mechanical parts elimination, improved compatibility with elevated generating power levels, and opportunities for integration of appealing new features such as active engine vibration damping. The system must deliver high power (60 kW) over a broad 10:1 engine speed range, and the machine torque requirements during starting to exceed those during generating operation by nearly a 2:1 ratio.

Consistent with this conclusion, a trade-off study of alternative brushless machine technologies revealed that the induction machine and interior permanent magnet machine offer the best promise for system cost optimization because of lower projected converter costs compared to their surface permanent magnet machine and variable reluctance machine rivals.

This same trade-off study indicated that the interior permanent magnet machine potentially offers some noteworthy advantages over the more established induction machine in such key areas as cost reduction by ferrite magnet material, and lower machine weight. The attractive torque density characteristics of the interior permanent magnet machine combined with its compatibility with wide ranges of constant power operation are primarily responsible for this positive trade-off assessment.

A decision was made to pursue the interior permanent magnet machine as a viable choice for the use of direct-drive alternators to determine whether these potential advantages can be realized. Achieving a satisfactorily high $L_q/L_d$ inductance ratio of 9 or higher is challenging in the face of magnetic saturation and the need to maintain high-speed mechanical integrity. This study is currently underway to find the best internal permanent magnet machine design that minimizes the total cost of the system without sacrificing any of the performance requirements. Finite element analysis tools are being aggressively applied to ensure that the nonlinear effects are being properly evaluated. Plans call for the construction and testing of a prototype alternator system following analytical verification of an acceptable design.

**References:**

[1]. Almansour, M. (2022). Electric vehicles (EV) and sustainability: Consumer response to twin transition, the role of e-businesses and digital marketing, *Technology in Society*, 71, 102135. Doi: 10.1016/j.techsoc.2022.102135

[2]. Xie, L., Luo, Y., Zhang, D., Chen, R., Li, K. (2019). Intelligent energy-saving control strategy for electric vehicle based on preceding vehicle movement, *Mechanical Systems and Signal Processing*, 130, 484-501. Doi: 10.1016/j.ymssp.2019.05.027

[3]. Sain, C., Banerjee, A., Biswas, P. K. (2020). Modelling and comparative dynamic analysis due to demagnetization of a torque controlled permanent magnet synchronous motor drive for energy-efficient electric vehicle, *ISA Transactions*, 97, 384-400. Doi: 10.1016/j.isatra.2019.08.008

[4]. He, H., Zhou, N., Sun, C. (2017). Efficiency decrease estimation of a permanent magnet synchronous machine with demagnetization faults, *Energy Procedia*, 105, 2718-2724. Doi: 10.1016/j.egypro.2017.03.922

[5]. Picot, A., Obeid, Z., Regnier, J., Poignant, S., Darnis, O., Maussion, P. (2014). Statistic-based spectral indicator for bearing fault detection in permanent-magnet synchronous machines using the stator current, *Mechanical Systems and Signal Processing*, *46*(2), 424-441. Doi: 10.1016/j.ymssp.2014.01.006

[6]. Arias, A., Ortega, C., Zaragoza, J., Espina, J., Pou, J. (2013). Hybrid sensorless permanent magnet synchronous machine four quadrant drive based on direct matrix converter, *International Journal of Electrical Power & Energy Systems*, *45*(1), 78-86. Doi: 10.1016/j.ijepes.2012.08.073

[7]. Pamuk, N. (2014). Statistical analysis of electrical and mechanical breakdown stress for insulation performance in high voltage power transformer, *Tehnicki vjesnik - Technical Gazette*, *21*(3), 495-503.

[8]. Wu, D., Jalal, A. S., Baker, N. (2017). A coupled model of the linear joule engine with embedded tubular permanent magnet linear alternator, *Energy Procedia*, *105*, 1986-1991. Doi: 10.1016/j.egypro.2017.03.571

[9]. Guo, C., Zuo, Z., Feng, H., Roskilly, T. (2021). Advances in free-piston internal combustion engines: A comprehensive review, *Applied Thermal Engineering*, 189, 116679. Doi: 10.1016/j.applthermaleng.2021.116679

[10]. Huber, J., Kopecek, H., Hofbaur, M. (2015). Nonlinear model predictive control of an internal combustion engine exposed to measured disturbances, *Control Engineering Practice*, *44*, 78-88. Doi: 10.1016/j.conengprac.2015.06.007

[11]. Yue, Q., Liu, G., Xu, Z., Xiong, D., Song, Z. (2022). Establishment the equivalent model and parameter calculation of a new concept of high-speed permanent magnet synchronous machine with hybrid excitation on the stator, *Energy Reports*, *8*(5), 815-824. Doi: 10.1016/j.egyr.2022.02.219

[12]. Widyan, M. S., Hanitsch, R. E. (2012). High-power density radial-flux permanent-magnet sinusoidal three-phase three-slot four-pole electrical generator, *International Journal of Electrical Power & Energy Systems*, *43*(1), 1221-1227. Doi: 10.1016/j.ijepes.2012.05.069

[13]. Mogenier, G., Baranger, T., Dufour, R., Besso, F., Durantay, L. (2011). Nonlinear centrifugal effects on a prestressed laminated rotor, *Mechanism and Machine Theory*, *46*(10), 1466-1491. Doi: 10.1016/j.mechmachtheory.2011.05.005

[14]. Han, X., Palazzolo, A. (2016). Unstable force analysis for induction motor eccentricity, *Journal of Sound and Vibration*, *370*, 230-258. Doi: 10.1016/j.jsv.2016.01.045